Check for updates

Fabrication and characterization of conductive electrospun nanofiber mats of carbon nanofiber/poly(vinyl alcohol)/poly(lactic acid) ternary nanocomposites for flexible electronics applications

Victor K Sharma, [†a] Gourhari Chakraborty,[b] Soundararajan Narendren[a] and Vimal Katiyar [*a]

Structural flexibility, high electrical conductivity, and biodegradability are some of the desired electrode properties required in electrode materials for various biomedical, biofuel cell, and flexible electronics applications. In this study, biodegradable polyvinyl alcohol (PVA) was covalently grafted onto surface-modified carbon nanofibers (mCFs) to form a highly conductive nanocomposite (PVA/mCF). This PVA/mCF nanocomposite was electrospun (PVA/mCF@PLA-es) or dip-coated (PVA/mCF@PLA) on neat polylactic acid (PLA) electrospun nanofiber mats to fabricate non-woven, flexible, and conductive nanofiber mats. The surface impedance of the PVA/mCF nanocomposite was reduced by 10^6 times compared to that of the neat polymer with no noticeable capacitance. Fourier transform infrared (FTIR) spectroscopy, Raman spectroscopy, X-Ray diffraction (XRD), and electron microscopy studies demonstrated evidence for successful surface modification of carbon nanofibers and covalent grafting of PVA. Thermogravimetric analysis (TGA) and contact angle studies also demonstrated improved thermal stability and wettability. Because of the excellent structural flexibility, high electrical conductivity, and biodegradability of PVA/mCF@PLA nanofiber mats, they could be used in biofuel cell electrodes, biomedical devices, and wearable electronics applications.

1 Introduction

Due to their diverse applications, conformability, and structural flexibility, flexible electronics have garnered ample attention from academic and industrial communities.[1–5] Flexible electronics encompass many applications, including wearable electronic devices, medical implants, flexible solar cells, flexible displays, thin film transistors, and flexible electrodes, and other applications involving energy storage, healthcare, and defense.[6–8] By the end of 2029, the commercial flexible electronics market globally is expected to surpass $77 billion at a compound annual growth rate of 8.5%.[9] The obvious choice of materials for achieving high electrical conductivity is metals. However, metals lack structural flexibility and thus are a poor choice for flexible electronics applications. Alternatives like transparent conductive metal oxides[10] and intrinsic conducting polymers[11] have also been studied exhaustively. Inherent challenges with metal oxides are that they are not structural materials and must be deposited on another substrate like glass or a polymer. Polymers with intrinsic conductivity, such as polyaniline, find common use in constructing gas sensors, supercapacitors, membranes, and fuel cell electrodes, as well as in applications like water purifiers and actuators.[12] Some polymers with conductivity possess acidic dopants and can potentially undermine the stability of the electronic apparatus in which they are employed.[13] For applications like medical implants[14] and microbial fuel cell electrodes,[15] essential properties are biocompatibility and biodegradability, mainly lacking in metals, metal oxides, and intrinsically conducting polymers.[8]

Electrically conductive composite materials based on biodegradable polymers like polyvinyl alcohol[16] and poly(lactic acid)[17] offer biocompatibility, biodegradability, and functionality. The advantage of a biocompatible, conductive, and polymer nanocomposite is that it can be used as a material for a

[a] Department of Chemical Engineering, Indian Institute of Technology Guwahati, North Guwahati, Assam 781039, India. E-mail: vkatiyar@iitg.ac.in

[b] Department of Chemical Engineering, National Institute of Technology Andhra Pradesh, Andhra Pradesh 534101, India

† Work was carried out at Indian Institute of Technology Guwahati, North Guwahati, India. Current affiliation of the first author is Department of Chemical and Petroleum Engineering, University of Kansas, Lawrence, Kansas 66045, USA.

multifaceted flexible electronics applications like wearable devices, biosensors, or flexible electrodes for microbial fuel cells. Polyvinyl alcohol (PVA) is an extensively researched natural polymer known for its strong biodegradability, favorable hydrophilic properties, and active alcohol-based side chain. These attributes make it an appropriate choice for creating nanocomposites alongside conductive additives like surface-modified carbon nanomaterials.[16,18] PVA-based nanofibers have shown promising results based on their unique surface properties for sophisticated, flexible electronics applications, like on-chip sensors.[19] Electrically conductive PVA hydrogels have been demonstrated for self-healing biosensor applications due to their excellent biocompatibility.

Carbon nanomaterials have become prominent constituents in the production of advanced composite materials intended for diverse electronics applications.[20,21] In these composite materials, carbon nanomaterials induce high electrical conductivity while a polymer matrix acts as the structural material while also providing bendability and conformability as required for flexible electronics applications.[4,22,23] Nanocomposites based on single-walled carbon nanotubes on polyethylene oxide nanofiber mats,[24] and poly(vinyl alcohol) nanofibers embedded with titanium nanoparticles[25] were demonstrated for biosensor and gas sensor applications, respectively. Among carbon nanomaterials, carbon nanotubes (CNTs) and 2-D graphene have been studied to a much greater extent than carbon nanofibers (CFs).[26] Although there is some ambiguity between carbon nanofiber and carbon fiber structural properties, Al-Saleh and Sundararaj showed that vapor-grown carbon nanofibers could have a diameter ranging between 50 nm and 200 nm (aspect ratio: 25–2000), while the carbon fiber diameter was 7.3 μm (aspect ratio: 440) and it shows almost 100 times lower thermal conductivity compared to carbon nanomaterials.[27] However, CFs have several advantages[28] over other carbon nanomaterials because of their facile synthesis, 100 times lower cost than single-walled carbon nanotubes,[29] equally superior electrical conductivity and ease of functionalization. A fundamental issue in incorporating carbon nanomaterials into polymer matrices is the insufficient interfacial interactions between the filler and the matrix, resulting in uneven dispersion of the nanomaterials.[30] In order to create high-performance nanocomposites using carbon nanomaterials such as graphene, carbon nanotubes (CNTs), and carbon nanofibers (CFs), it is necessary to perform functionalization of these materials before introducing them into a polymer matrix.[31] Utilizing covalent functionalization of carbon nanomaterials could be an effective strategy for creating nanocomposites where carbon nanomaterials are grafted onto a polymer matrix. It facilitates filler–matrix compatibility by promoting adhesion between the carbon nanomaterial and polymer to achieve superior functional properties.[32–35]

Electrodes required to have high electrochemical surface area and structural flexibility for their application in flexible electronics devices. Electrospinning has been used as a popular choice for producing flexible, non-woven nanofibers with high electrochemical surface area for applications requiring high electrical conductivity.[25,36,37] This unique method utilizes straightforward instrumentation, leveraging a high-voltage electric field to guide a polymer solution into a stable jet formation, leading to the creation of nanofiber mats spanning a range from a few micrometers to several nanometers in the fiber diameter.

Although polymer nanocomposites have been synthesized and characterized for various applications, evidence for combined properties, including electrical conductivity, flexibility, biocompatibility and biodegradability, is still lacking in the literature. This study aims to synthesize and characterize a biodegradable, biocompatible polymer-based electrically conductive nanocomposite for flexible electronics applications. CFs were functionalized to generate acyl chloride moieties on their surface. The modified CFs (mCFs) were used as conductive fillers in the PVA matrix using a covalent grafting technique to enhance filler–matrix interactions to synthesize an electrically conductive nanocomposite (PVA/mCF). The electrospinning technique was used to fabricate flexible electrospun nanofiber mats using polylactic acid (PLA) solutions with chloroform as the solvent. PVA/mCF was then incorporated into the PLA nanofiber mats using two different methods. In the first method, PVA/mCF with various weight percentages of mCFs was directly electrospun from its aqueous solutions on the PLA nanofiber mats. The second method used PVA/mCF glycol solution to dip-coat[38] the PLA mats to fabricate flexible, conductive nanofiber mats. Several characterization techniques were employed to understand and analyze the influence of CF composition dispersion and fabrication techniques on the nanofiber mats' surface and thermal and electrical properties. These highly flexible, biocompatible and electrically conductive nanofiber mats can be used in a wide range of flexible electronics applications.

2 Experimental section

2.1 Materials and chemicals

Polyvinyl alcohol (PVA) with a molecular weight ranging from 89 000 Da to 98 000 Da was procured from Sigma Aldrich and utilized without additional purification. Vapor-grown carbon nanofibers, exhibiting an intrinsic impedance of 0.005 Ω, were acquired from Sigma Aldrich and used as is. Poly(L-lactic acid) (PLA) of 2003D grade from NatureWorks® LLC (USA) was employed without modification. Other analytical-grade reagents, including thionyl chloride ($SOCl_2$), nitric acid (HNO_3), sulfuric acid (H_2SO_4), chloroform ($CHCl_3$), and ethylene glycol ($C_2H_6O_2$), were used in the study.

2.2 Surface modification of CFs

To produce oxidized carbon fibers with carboxylic acid groups (CF–COOH), 300 mg of carbon fibers (CF) was combined with 200 ml of a mixture of 3 : 1 v/v of concentrated nitric acid and sulfuric acid. The mixture was heated in a 500 ml round bottom flask at 120 °C, under constant reflux and stirring at 600 rpm for 45 minutes. Following this, the resulting product was allowed to settle, and the acid was removed through repeated
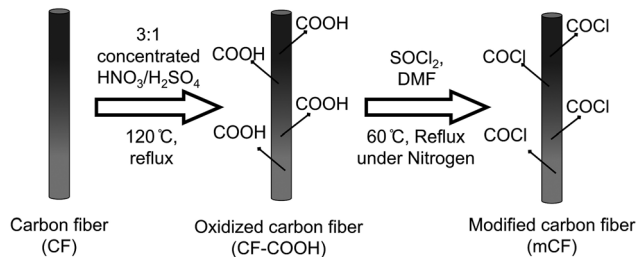
Scheme 1 Schematic representation of the surface modification of CFs.

Scheme 2 Representation of the electrospinning setup used to synthesize nanofiber mats.

sedimentation and decantation using deionized (DI) water. CF–COOH was subsequently subjected to centrifugation and washed multiple times to eliminate most of the residual acid. The product was then dialyzed using a cellulose acetate membrane until the pH approached a value near 7.

In the next step, 100 mg of dried CF–COOH was mixed with 30 ml of thionyl chloride ($SOCl_2$), and 2 ml of dimethylformamide (DMF) was introduced as a catalyst in a round bottom flask. This setup was placed in an oil bath at 60 °C with constant stirring at 600 rpm and nitrogen gas purging for 24 hours. The resulting product was meticulously washed using tetrahydrofuran (THF) until all unreacted $SOCl_2$ was eliminated. The washed product underwent further centrifugation and washing steps with water, followed by pH adjustment using a membrane dialysis bag and deionized water. The process concluded with vacuum drying at 60 °C for 2 days to obtain the surface-modified carbon fiber (mCF), as depicted in Scheme 1.

2.3 Covalent grafting of mCFs on PVA

To initiate the covalent grafting procedure, 120 mg of polyvinyl alcohol (PVA) was dissolved in an excess of water. Subsequently, 7.6 mg, 10.4 mg, 13.3 mg, or 30 mg of surface-modified carbon fiber (mCFs) was incorporated into this solution. The mixture was subjected to sonication using a probe sonicator for a duration of 2 hours, resulting in the creation of PVA/mCF composites with varying weight percentages: 6%, 8%, 10%, and 20%, denoted as PVA/mCF-6, PVA/mCF-8, PVA/mCF-10, and PVA/mCF-20, respectively. The resultant dispersions were then heated under reflux at 80 °C for a duration of 3 hours. Following this step, the products were centrifuged to eliminate excess water. The resulting samples were subsequently freeze-dried to yield the dried grafted PVA/mCF nanocomposites. In the rest of this article, PVA/mCF-20 is referred to as PVA/mCF.

2.4 Fabrication of conductive nanofiber mats

The solution for electrospinning polylactic acid (PLA) was created by dissolving 2 g of pure PLA in 10 ml of 3 : 1 chloroform and dimethylformamide (DMF) mixture (v/v). This solution was stirred continuously overnight. Subsequently, the resulting PLA solution was subjected to electrospinning to produce a nanofiber mat of neat PLA (PLA-es). This process was carried out on an oscillating plate as the collector (Scheme 2) to obtain a large area of the electrospun nanofiber using the following parameters: a syringe with a diameter of 13.6 mm, an interelectrode distance of 13 cm, a flow rate of 1 ml h^{-1}, and
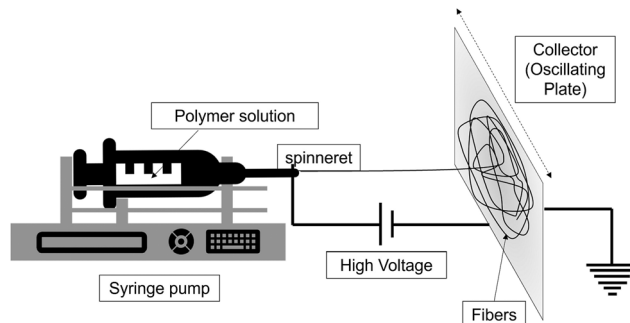
an applied voltage of 6.5 kV. The PLA nanofiber mat was subsequently dried overnight in a hot-air oven at 50 °C.

2.4.1. Electrospinning of PVA/mCFs on the neat PLA nanofiber mat. PVA/mCF-6, PVA/mCF-8, PVA/mCF-10, and PVA/mCF-20 were dissolved in water to form a 20% (w/V) solution and electrospun on top of the neat PLA nanofiber mat to fabricate conductive nanofiber mats PVA/mCF-6@PLA-es, PVA/mCF-8@PLA-es, PVA/mCF-10@PLA-es, and PVA/mCF-20@PLA-es, respectively.

2.4.2 Dip-coating process for PVA/mCF on the PLA nanofiber mat. The dried nanocomposite of PVA/mCF was dissolved in ethylene glycol to produce a 10% (w/v) solution. The PLA nanofiber mat was sectioned into pieces measuring 1 cm × 5 cm. These pieces were subjected to a dip-coating process,[39] where they were immersed in the 10% (w/v) PVA/mCF solution in ethylene glycol (Scheme 3). Subsequently, the coated pieces were left to dry in a hot-air oven at 50 °C overnight. The outcome was a flexible, conductive nanofiber mat (PVA/mCF@PLA) that served as the final material for the electrode.

2.5 Characterization techniques

2.5.1 Fourier transform infrared (FTIR) studies. FTIR spectroscopy of CF, CF–COOH, and mCFs; PVA and PVA/mCF was carried out to confirm the surface modification of CFs and the polymer grafting on the mCF surface, respectively. The samples were thoroughly combined with KBr of high purity (>99%) and subsequently examined in the form of pellets
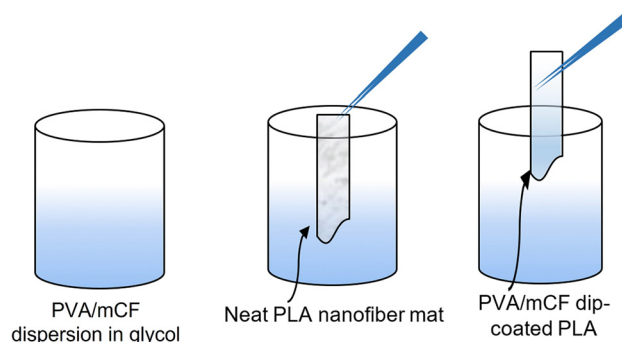
Scheme 3 Representation of the dip-coating process for PVA/mCF@PLA fabrication.

using a PerkinElmer FTIR spectrometer, covering a wavenumber range spanning from 4000 to 500 cm^{-1}.

2.5.2 Raman spectroscopy studies. Raman analysis of CF, CF–COOH, PVA, and PVA/mCF was performed using a spectrometer (Horiba Jobin Yvon, Model: Lab Ram HR) fitted with an Nd:YAG diode-pumped laser (1 W, 1064 nm). The excitation wavelength was set at 633 nm. The samples were scanned across a wavenumber range from 3000 to 500 cm^{-1}.

2.5.3 Thermal degradation studies. A PerkinElmer TGA4000 thermogravimetric analyzer was used to collect the thermal degradation patterns of PVA, CFs and PVA/mCF. The specimens, weighing (7.5 ± 0.3) mg, were subjected to thermogravimetric analysis (TGA) over a temperature range of 25 to 700 °C with a heating rate of 10 °C min^{-1}. A flow of nitrogen gas at 20 mL min^{-1} was maintained to ensure an inert atmosphere throughout the analysis.

2.5.4 X-ray diffraction (XRD) studies. The diffraction profiles for CFs, mCFs, PVA, and PVA/mCF were acquired using a Bruker D8 diffractometer. The measurements were performed under ambient conditions and room temperature, utilizing a Cu-Kα radiation source (λ = 0.15406 nm). The instrument was set at 40 kV and 40 mA for the duration of the analysis. The diffraction data were collected with a step duration of 0.5 s, scanning within a 2θ range of 1 to 60 degrees and a scanning speed of 0.05 s^{-1}.

2.5.5 Morphological studies. The surface characteristics of CF, mCFs, PVA/mCF, and PLA, as well as PVA/mCF@PLA nanofibers, were examined using a Zeiss Sigma 300 field emission scanning electron microscope (FESEM) equipped with an in-lens secondary electron (SE) detector. Prior to imaging, the samples were coated with a thin layer of gold through sputtering for 180 seconds. Additionally, the morphology of PVA/mCF was investigated using a JEOL 2100F transmission electron microscope (TEM). For TEM analysis, samples were prepared by applying a solution of PVA/mCF onto a TEM grid coated with a carbon layer.

2.5.6 Wettability studies. Contact angle analysis was employed to investigate the wettability of PLA and PVA/mCF@PLA nanofiber mats. This analysis was conducted using a KRUSS goniometer through the sessile-drop method. Three points on each sample were assessed for contact angle measurements, and the average angle was recorded. Measurements were taken 60 seconds after dispensing a 5 μL water droplet from an injector.

2.5.7 Electrochemical impedance spectroscopy (EIS) studies. The impedance characteristics of the 1 cm × 5 cm electrospun nanofiber mats of PVA/mCF-6@PLA-es, PVA/mCF-10@PLA-es, PVA/mCF-20@PLA-es, and PVA/mCF@PLA were assessed using a Metrohm Autolab potentiostat instrument and a four-point-probe method (Fig. 1).[40] A potentiostatic frequency response analysis was conducted across a range of 0.1 to 10^6 Hz, compared to the impedance measurements conducted at frequencies of 0.1, 10, and 21,544 Hz.

2.5.8 Current–voltage (I–V) response studies. Cyclic voltammetry (CV) was employed to analyze the current–voltage (I–V) characteristics. The measurements were conducted using a
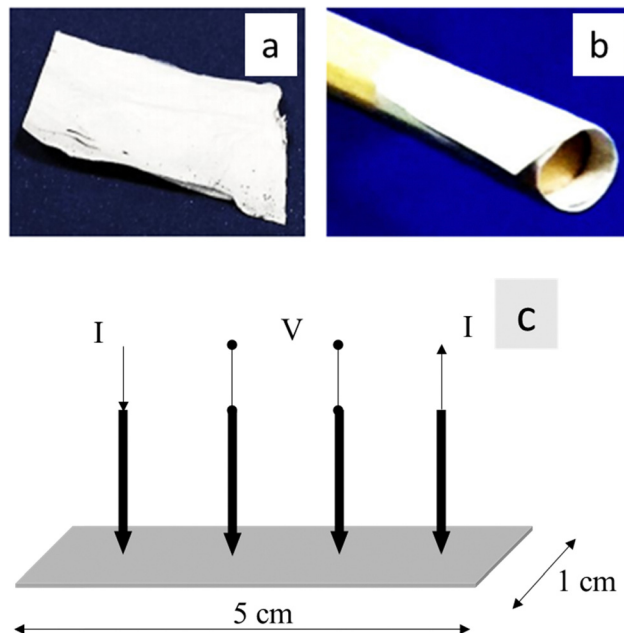

Fig. 1 (a) and (b) 1 cm × 5 cm strip of PVA/mCF@PLA flexible nanofiber mats, (c) schematic of a 4-point probe method for impedance measurement.

three-electrode system and an Autolab PGSTAT 204 instrument manufactured by Metrohm India Ltd.[41] For the working electrode, a segment of the PVA/mCF@PLA nanofiber mat, measuring 1 cm × 5 cm, was utilized against an Ag/AgCl reference electrode and a platinum counter electrode in a 1 M KOH aqueous electrolyte solution. Twenty-five scans were conducted with a scan rate of 100 mV s^{-1}. The initiation and termination potentials were both set at −1.00 V. The range was bounded by upper and lower vertex potentials of 1.00 V and −1.005 V, correspondingly, and the step potential was set at 0.002 V.

3 Results and discussion

3.1 Fourier transform infrared (FTIR) studies

Fig. 2 illustrates the FTIR spectra of CFs, CF–COOH, mCFs, PVA, and PVA/mCF. The peaks at 1564 cm^{-1} and 1418 cm^{-1} signify the skeletal vibration of the carbon fiber. The range from 3276 cm^{-1} to 3600 cm^{-1} corresponds to the –OH stretching vibration attributed to moisture in the CFs. Upon oxidation, this –OH stretching vibration intensity was higher due to the presence of the (–COOH) moiety in CF–COOH compared to CFs.[42] The concomitant appearance of a peak ~1700 cm^{-1} could be attributed to C=O stretching vibration, which indicates the formation of –COOH and –COCl groups in CF–COOH and mCFs, further confirming successful partial surface functionalization of CFs. Furthermore, the peak due to –OH stretching vibrations experienced a slight shift to 3520 cm^{-1} due to the transformation of –COOH groups into –COCl in the mCF spectrum. The emergence of a peak at 771 cm^{-1} was attributed to the C–Cl bond stretching vibrations, confirming

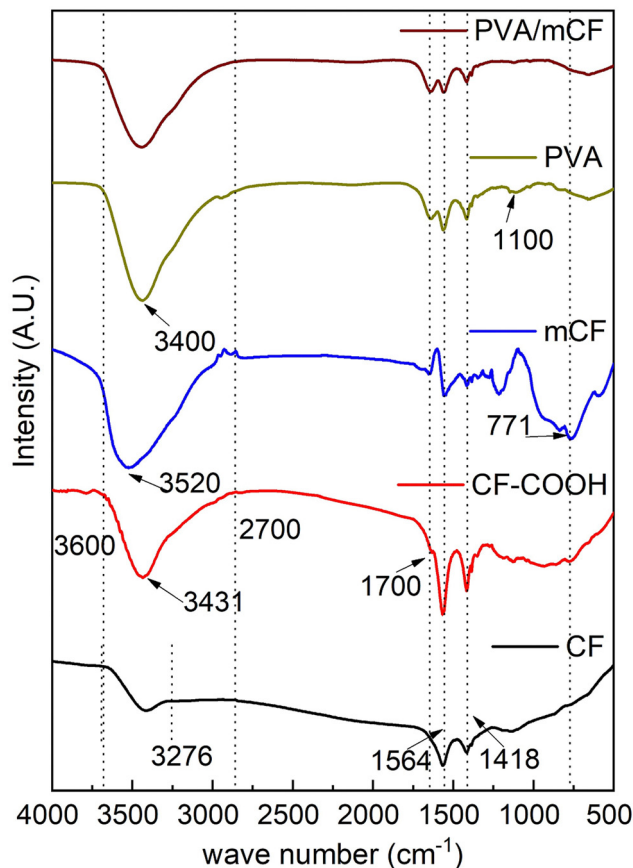Fig. 2 Infrared spectra of CFs, CF-COOH, mCFs, PVA, and PVA/mCF (bottom-up).

Fig. 3 Raman spectra of CFs, CF–COOH, PVA, and PVA/mCF (bottom-up).

the successful modification of CF. In the PVA spectrum, the peak at 1564 cm^{-1} originates from the stretching vibrations of C–H in the PVA backbone, and a robust hydroxyl stretching vibration peak is noticeable at 3400 cm^{-1}. The peak at 1100 cm^{-1} is linked to C–OH bond stretching, an attribute not observed in the PVA/mCF spectrum. The simultaneous absence of the C–Cl peak at 771 cm^{-1} verifies the effective grafting of PVA onto mCFs.

3.2 Raman spectroscopy studies

Fig. 3 shows the Raman spectra of CFs, CF–COOH, PVA, and PVA/mCF. At Raman shifts of 1578 cm^{-1} and 1319 cm^{-1}, the D and G bands represent distinctive CF characteristics.[39] The ratios of the intensities of the D band (I_D) and G band (I_G) for CF and CF–COOH are tabulated in Table 1. It should be noted that the I_D/I_G ratio of CFs escalated from 0.92 to 1.11 in CF–COOH. This notable increase in the I_D/I_G ratio within the oxidized carbon fiber CF-COOH indicates a transformation of graphitic sp^2 carbon into sp^3 carbon during CF oxidation. This, in turn, generates defects on the exposed graphene edges on the CF surface, resulting in the emergence of surface –COOH functional groups.[16] In the PVA spectra, prominent bands associated with polyvinyl alcohol were observed at 1444 cm^{-1} and 2915 cm^{-1}, corresponding to shear mode and C–H

vibrations, respectively.[43] The presence of graphitic peaks in the PVA/mCF spectrum further corroborates the successful grafting of PVA onto the mCF surface.

3.3 X-ray diffraction (XRD) studies

Fig. 4 presents the X-ray diffraction (XRD) profiles of CFs, mCFs, PVA and PVA/mCF. It was observed that the peaks at 2θ values of 26.1, 42.9, and 44.8 degrees were similar to the characteristic peaks of graphite, corresponding to the planes 002, 100, and 101, respectively.[44] In the mCF XRD pattern, a slight broadening of the peak at $2\theta = 26.1$ degrees was observed, which could be attributed to a minor reduction in crystallinity resulting from the conversion of some sp^2 carbon into sp^3 carbon. However, despite this, the identical peak position suggests that the primary crystalline structure of CFs remained unchanged after modification into mCFs. Notably, PVA's characteristic peaks emerged at 2θ values of 19.8 and 22.9 degrees. In the XRD pattern of PVA/mCF, incorporation of graphitic peak at $2\theta = 26.1$ degrees was evident, offering further confirmation of the successful grafting of PVA onto the mCF surface, with effective mCF dispersion. Additionally, the concurrent broadening of the PVA's signature peak at

Table 1 Comparison of I_D/I_G ratios of CFs and CF–COOH

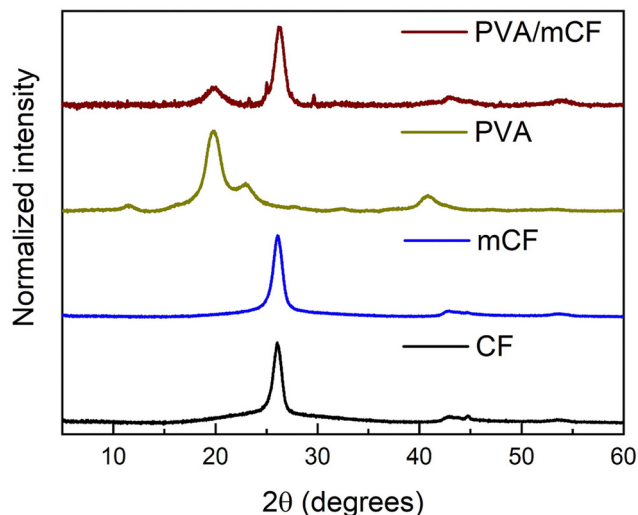| Sample	I_D	I_G	I_D/I_G
CF	120.7	130.7	0.9
CF–COOH	264.3	238.8	1.1

Fig. 4 XRD patterns of CFs, mCFs, PVA, and PVA/mCF (bottom-up).

$2\theta = 19.8$ degrees indicated a reduction in PVA's inherent crystallinity upon its grafting onto mCFs.

3.4 Thermal degradation studies

Thermogravimetric analysis (TGA) curves for PVA, mCFs and the PVA/mCF nanocomposite are shown in Fig. 5. The inset plot shows the differential weight loss *versus* the temperature of PVA and PVA/mCF. It was observed that the mass loss of mCFs was below 7%, primarily due to the thermal decomposition of surface functional groups and some moisture present in the mCF. The analysis of PVA's thermal degradation profile revealed the presence of approximately 3% moisture content, which was observed to evaporate between 25 and 100 °C. The differential weight loss curve indicated a two-stage thermal decomposition of PVA, occurring at around 300 °C and 460 °C.
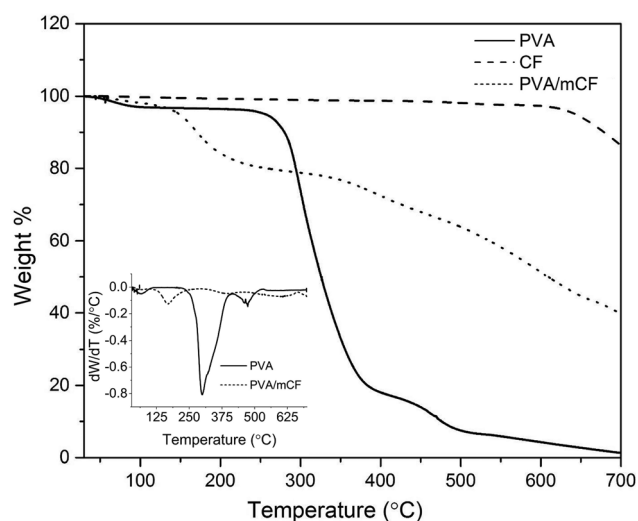
Fig. 5 TGA curves of PVA, CFs, and the PVA/mCF nanocomposite. The inset plot depicts differential weight loss of PVA and PVA/mCF with temperature.

Most of the weight loss transpired below 500 °C, with only about 2% residual weight remaining for PVA.

In the PVA/mCF nanocomposite, a gradual weight loss was noted below 100 °C, attributed to the presence of moisture in the composite. A distinct weight loss gradient emerged at 150 °C, possibly due to portions of the PVA matrix that were not covalently bonded to the mCF surface. As the temperature increased, the thermal decomposition of PVA/mCF was significantly delayed due to the robust covalent linkage between the surface-modified carbon fiber (mCF) and the polymer matrix (PVA). Remarkably, the PVA/mCF exhibited a residual weight of approximately 39% at 700 °C, a nearly twenty-fold increase compared to pristine PVA. This suggests that the thermal stability of the covalently grafted PVA/mCF nanocomposite was significantly enhanced, rendering it suitable for high-temperature applications like thermocouples. A similar finding was reported by Malikov *et al.*,[16] wherein the thermal degradation pattern of PVA-grafted MWCNT nanocomposites demonstrated enhanced thermal stability due to covalent grafting.

3.5 Morphological studies

Fig. 6(a)–(c) show the scanning electron micrographs of unmodified CFs, mCFs and PVA/mCF. The diameter distribution of CF fibers spanned from 100 to 200 nanometers, exhibiting a relatively smooth surface. In contrast, significant surface roughness was evident in mCFs, as depicted in Fig. 6b, possibly arising from the defects introduced during CF surface modification. Furthermore, the interweaving of carbon fibers within the PVA-grafted carbon fiber matrix is distinctly visible in Fig. 6c. This observation underscores the notable compatibility between the mCFs as a filler and the PVA matrix, further corroborated by the entanglement pattern seen in the micrograph. The neat PLA electrospun nanofiber mat (PLA-es) was characterized by larger diameters ranging between 500 and 1200 nm (Fig. 6d). The PVA/mCF-20@PLA-es electrospun nanofiber mat is shown in Fig. 6e, where the surface layer of electrospun PVA/mCF with smaller diameters is visible above the underlying electrospun PLA layer. The dip-coated PVA/mCF@PLA nanofiber mat consisted of a surface film of PVA/mCF; hence, high-resolution micrographs could not be obtained for this sample. Transmission electron micrographs further showed the PVA/mCF morphology, and a heavily cross-linked mCF network was observed due to the covalent grafting of PVA (Fig. 6f). Certain mCF instances displayed multiple PVA patches distributed along their length, while others exhibited a consistent coating, leading to a slight augmentation in the fiber diameter. Xu *et al.*[45] observed a similar increase in the MWCNT diameter due to the deposition of amorphous layers of poly-(*N-iso*-propyl acrylamide) when covalently grafted onto MWCNTs. Altogether, morphological evidence for successful surface modification of CFs and covalent grafting of PVA on mCFs was observed in scanning and transmission electron micrographs. Therefore, the covalent grafting strategy could be deemed reliable for fabricating polymer-based conductive nanofiber mats.
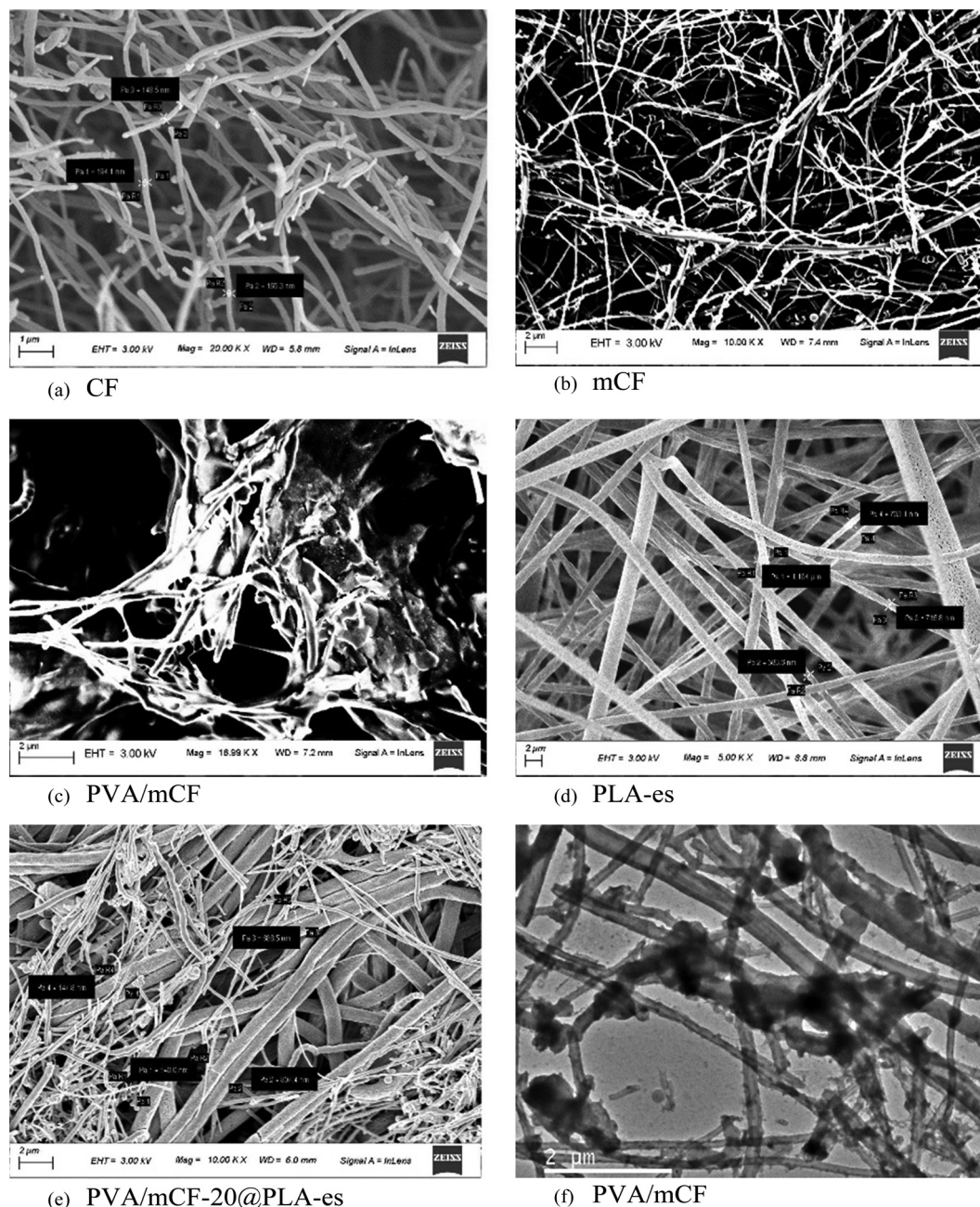
(a) CF

(b) mCF

(c) PVA/mCF

(d) PLA-es

(e) PVA/mCF-20@PLA-es

(f) PVA/mCF

Fig. 6 (a)–(e) Scanning electron micrographs of CFs, mCFs, PVA/mCF, neat PLA nanofiber mats, and PVA/mCF@PLA-es nanofiber mats, respectively; (f) transmission electron micrograph of PVA/mCF.

3.6 Wettability studies

The contact angle of neat PLA-es nanofiber mats was equal to $(130 \pm 6)°$ due to their hydrophobic characteristics (Fig. 7a). The dip-coated PVA/mCF@PLA nanofiber mats had a contact angle of $(74 \pm 15)°$ (Fig. 7b), almost decreased by 43% compared to the neat PLA-es nanofiber mats. The decrease in the contact angle can be attributed to PVA's inherent hydrophilicity and the augmented hydrophilic properties of mCFs compared to CFs, brought about by the presence of surface functional groups. The elevated standard deviation may be attributed to the uneven surface and inconsistent thickness of the PVA/mCF
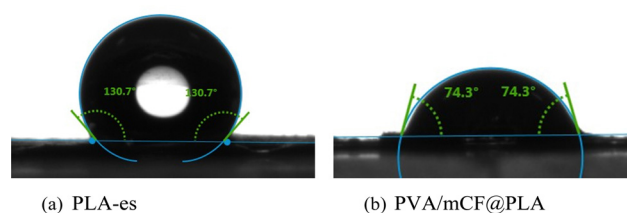
(a) PLA-es

(b) PVA/mCF@PLA

Fig. 7 Contact angles of (a) neat PLA electrospun nanofiber mats (PLA-es), (b) dip-coated PVA/mCF on PLA nanofiber mats (PVA/mCF@PLA).

contributed to review and editing. G.C and N.S contributed to investigations, formal analyses, reviews and editing. V.K was responsible for conceptualizing the study, funding acquisition, managing project administration, providing supervision, and contributing to review and editing.

Conflicts of interest

The authors declare no conflicts of interest.

Acknowledgements

References

1 H. R. Ansari, A. Mirzaei, H. Shokrollahi, R. Kumar, J.-Y. Kim, H. W. Kim, M. Kumar and S. S. Kim, *J. Mater. Chem. C*, 2023, **11**, 6528–6549.
2 A. Chinnappan, C. Baskar, S. Baskar, G. Ratheesh and S. Ramakrishna, *J. Mater. Chem. C*, 2017, **5**, 12657–12673.
3 A. H. Espera, J. R. C. Dizon, A. D. Valino and R. C. Advincula, *Jpn. J. Appl. Phys.*, 2022, **61**, SE0803.
4 C. Jellett, K. Ghosh, M. P. Browne, V. Urbanová and M. Pumera, *ACS Appl. Energy Mater.*, 2021, **4**, 6975–6981.
5 D. Ye, Y. Ding, Y. Duan, J. Su, Z. Yin and Y. A. Huang, *Small*, 2018, **14**, 1703521.
6 G. Zhou, F. Li and H.-M. Cheng, *Energy Environ. Sci.*, 2014, **7**, 1307–1338.
7 S. Park, M. Vosguerichian and Z. Bao, *Nanoscale*, 2013, **5**, 1727–1752.
8 D.-L. Wen, D.-H. Sun, P. Huang, W. Huang, M. Su, Y. Wang, M.-D. Han, B. Kim, J. Brugger, H.-X. Zhang and X.-S. Zhang, *Microsyst. Nanoeng.*, 2021, **7**, 1–25.
9 Flexible, Printed and Organic Electronics 2019–2029: Forecasts, Players & Opportunities, 2018.
10 M. R. Akanda, A. M. Osman, M. K. Nazal and M. A. Aziz, *J. Electrochem. Soc.*, 2020, **167**, 037534.
11 V. Babel and B. L. Hiran, *Polym. Compos.*, 2021, **42**, 3142–3157.
12 Y. Wang, *Polym. Int.*, 2018, **67**, 650–669.
13 W. Lee, M. Song, S. Park, S. Nam, J. Seo, H. Kim and Y. Kim, *Sci. Rep.*, 2016, **6**, 33795.
14 E. W. Lau, in *Clinical Cardiac Pacing, Defibrillation and Resynchronization Therapy*, ed. K. A. Ellenbogen, B. L. Wilkoff, G. N. Kay, C.-P. Lau and A. Auricchio, Elsevier, 2017, pp. 313–351.e29.
15 K. Guo, PhD dissertation, Ghent University, 2014.
16 E. Y. Malikov, M. B. Muradov, O. H. Akperov, G. M. Eyvazova, R. Puskás, D. Madarász, L. Nagy, Á. Kukovecz and Z. Kónya, *Phys. E*, 2014, **61**, 129–134.

17 G. Chakraborty, P. Dhar, V. Katiyar and G. Pugazhenthi, *J. Mater. Sci.: Mater. Electron.*, 2020, **31**, 5984–5999.
18 S. Gahlot, V. Kulshrestha, G. Agarwal and P. K. Jha, *Macromol. Symp.*, 2015, **357**, 173–177.
19 Z.-C. Chen, T.-L. Chang, T.-C. Pan, D. Chiang and S.-F. Tseng, *Mater. Lett.*, 2018, **233**, 130–133.
20 G. Chakraborty, G. Pugazhenthi and V. Katiyar, *Polym. Bull.*, 2019, **76**, 2367–2386.
21 M. Moniruzzaman and K. I. Winey, *Macromolecules*, 2006, **39**, 5194–5205.
22 B. Li, F. Zhang, S. Guan, J. Zheng and C. Xu, *J. Mater. Chem. C*, 2016, **4**, 6988–6995.
23 Z. Yu, X. Niu, Z. Liu and Q. Pei, *Adv. Mater.*, 2011, **23**, 3989–3994.
24 Y. Liu, J. Chen, N. T. Anh, C. O. Too, V. Misoska and G. G. Wallace, *J. Electrochem. Soc.*, 2008, **155**, K100.
25 G. F. El Fawal, H. S. Hassan, M. R. El-Aassar and M. F. Elkady, *Arabian J. Sci. Eng.*, 2019, **44**, 251–257.
26 L. Wen, F. Li and H.-M. Cheng, *Adv. Mater.*, 2016, **28**, 4306–4337.
27 M. H. Al-Saleh and U. Sundararaj, *Composites, Part A*, 2011, **42**, 2126–2142.
28 L. Guo, K. Wan, B. Liu, Y. Wang and G. Wei, *Nanotechnology*, 2021, **32**, 442001.
29 I. Kang, Y. Y. Heung, J. H. Kim, J. W. Lee, R. Gollapudi, S. Subramaniam, S. Narasimhadevara, D. Hurd, G. R. Kirikera, V. Shanov, M. J. Schulz, D. Shi, J. Boerio, S. Mall and M. Ruggles-Wren, *Composites, Part B*, 2006, **37**, 382–394.
30 P.-C. Ma, N. A. Siddiqui, G. Marom and J.-K. Kim, *Composites, Part A*, 2010, **41**, 1345–1367.
31 V. D. Punetha, S. Rana, H. J. Yoo, A. Chaurasia, J. T. McLeskey, M. S. Ramasamy, N. G. Sahoo and J. W. Cho, *Prog. Polym. Sci.*, 2017, **67**, 1–47.
32 V. T. Le, C. L. Ngo, Q. T. Le, T. T. Ngo, D. N. Nguyen and M. T. Vu, *Adv. Nat. Sci.: Nanosci. Nanotechnol.*, 2013, **4**, 035017.
33 J. Qiu, J. Li, Z. Yuan, H. Zeng and X. Chen, *Appl. Compos. Mater.*, 2018, **25**, 853–860.
34 N. Wang, S. Pandit, L. Ye, M. Edwards, V. R. S. S. Mokkapati, M. Murugesan, V. Kuzmenko, C. Zhao, F. Westerlund, I. Mijakovic and J. Liu, *Carbon*, 2017, **111**, 402–410.
35 N. Raphael, K. Namratha, B. N. Chandrashekar, K. K. Sadasivuni, D. Ponnamma, A. S. Smitha, S. Krishnaveni, C. Cheng and K. Byrappa, *Prog. Cryst. Growth Charact. Mater.*, 2018, **64**, 75–101.
36 Y. Zhang and G. C. Rutledge, *Macromolecules*, 2012, **45**, 4238–4246.
37 J. P. F. Santos, M. Arjmand, G. H. F. Melo, K. Chizari, R. E. S. Bretas and U. Sundararaj, *Mater. Des.*, 2018, **141**, 333–341.
38 S. Sugumaran, C. S. Bellan, D. Muthu, S. Raja, D. Bheeman and R. Rajamani, *RSC Adv.*, 2015, **5**, 10599–10610.
39 C.-H. Park, C.-H. Kim, L. D. Tijing, D.-H. Lee, M.-H. Yu, H. R. Pant, Y. Kim and C. S. Kim, *Fibers Polym.*, 2012, **13**, 339–345.
40 D. K. Schroder, *Semiconductor Material and Device Characterization*, John Wiley & Sons, Ltd, 2005.

41 N. Elgrishi, K. J. Rountree, B. D. McCarthy, E. S. Rountree, T. T. Eisenhart and J. L. Dempsey, *J. Chem. Educ.*, 2018, **95**, 197–206.

42 A. Fraczek-Szczypta, E. Menaszek, T. B. Syeda, A. Misra, M. Alavijeh, J. Adu and S. Blazewicz, *J. Nanopart. Res.*, 2012, **14**, 1181.

43 C. F. P. de Oliveira, P. A. R. Muñoz, M. C. C. dos Santos, G. S. Medeiros, A. Simionato, D. A. Nagaoka, E. A. T. de Souza, S. H. Domingues and G. J. M. Fechine, *Polym. Compos.*, 2019, **40**, E312–E320.

44 R. Das, S. B. A. Hamid, M. E. Ali, S. Ramakrishna and W. Yongzhi, *Curr. Nanosci.*, 2015, **11**(1), 23–35.

45 G. Xu, W.-T. Wu, Y. Wang, W. Pang, P. Wang, Q. Zhu and F. Lu, *Nanotechnology*, 2006, **17**, 2458.

46 Z. Yang, X. Li, J. Si, Z. Cui and K. Peng, *J. Wuhan Univ. Technol., Mater. Sci. Ed.*, 2019, **34**, 207–215.

47 M. Kosmulski, P. Próchniak and C. Saneluta, *Adsorption*, 2009, **15**, 172–180.